Field measurements on spatial variations in aeolian sediment availability at the Sand Motor mega nourishment

Hoonhout, Bas; de Vries, Sierd

Important note
To cite this publication, please use the final published version (if applicable).
Please check the document version above.

1 # Field Measurements on Spatial Variations in Aeolian
2 # Sediment Availability at the Sand Motor Mega
3 # Nourishment

4 **Abstract**

Spatial variations in aeolian sediment transport were measured at the Sand Motor mega nourishment in The Netherlands during a six week field campaign in the fall of 2014. A consistent significant increase in sediment transport in downwind direction (positive gradient) was measured over the intertidal beach area, indicating that the intertidal beach is a primary source of aeolian sediment, despite the high soil moisture contents. A small positive increase in transport in downwind direction was measured over the dry beach, indicating that local aeolian sediment supply was hampered. A consistent decrease in sediment transport in downwind direction (negative gradient) was measured at the transition between intertidal and dry beach, indicating local deposition of sediment. The negative gradients coincide with the berm edge and the onset of a shell pavement. Therefore deposition might be promoted by morphological feedback between a berm and the wind and the entrapment of sediment in the beach armor layer. The local sediment deposits cause the sediment supply to the dunes to be continued even during high water, resulting in a phased process. The influence of the beach armor layer reduces during storm events as the armor layer itself is being mobilized.

5 *Keywords:* aeolian transport; transport gradients; sediment availability;
6 sediment supply; beach armoring; field measurements; nourishments; Sand
7 Motor

1. Introduction

The Sand Motor (or Sand Engine) is an innovative solution to counteract the anticipated coastal recession due to sea level rise (Stive et al., 2013). The Sand Motor is a 21 Mm^3 mega nourishment along the Dutch coast that is constructed well above storm surge level and therefore largely shaped by wind. While the Sand Motor accommodates fetches up to 1.0 km and is permanently exposed to wind, the dry surface area is remarkably stable (Hoonhout and de Vries, 2016a). An armor layer consisting of shells, pebbles and cobbles prevent erosion by wind and thus limit the sediment availability (following the definition of Kocurek and Lancaster, 1999). Consequently, the aeolian sediment transport rates at the Sand Motor are limited to approximately 35% of the wind transport capacity (Hoonhout and de Vries, 2016a) making the Sand Motor an availability-limited coastal system.

In an availability-limited coastal system, not the wind transport capacity, but the sediment availability governs the sediment supply towards the dunes (Houser and Ellis, 2013). Sediment availability can be limited by various bed surface properties, like shells, salt crusts, moisture and vegetation. Studies on the influence of bed surface properties on aeolian sediment availability and transport started as wind tunnel experiments (e.g. Belly, 1964; Howard, 1977; Dyer, 1986; Gillette and Stockton, 1989). These studies typically determine an adapted threshold velocity that relates the theoretical wind transport capacity to a measured sediment transport capacity (Bagnold, 1937). In the field, the influence of different bed surface properties on sediment availability cannot easily be distinguished and the sediment availability is often presented spatially aggregated (Jackson and Nordstrom, 1998; Arens et al., 2001; Wiggs et al., 2004). The concept of critical fetch is a widely used approach for spatial aggregation of sediment supply (e.g. Jackson and Cooper, 1999; Davidson-Arnott et al., 2005, 2008; Bauer et al., 2009). The critical fetch is the distance over which the saltation cascade develops and aeolian sediment transport becomes saturated (Bauer and Davidson-Arnott, 2002). Since the saltation cascade develops slower when sediment is scarce, the critical fetch is inversely proportional to the sediment supply (Delgado-Fernandez, 2010).

Expressing the sediment supply in terms of critical fetch assumes that saturated transport is reached if the available fetch is sufficient. Hoonhout and de Vries (2016a) showed that sediment supply can be severely limited even with fetches as large as at the Sand Motor. Consequently, critical fetches may become very large or even undefined and the definition and interpretation of the critical fetch impractical (Lynch et al., 2016; de Vries et al., 2014a). Moreover, significant spatial variations in sediment supply were found in the Sand Motor region that challenges the spatial aggregation of sediment availability.

2

Alternatively, aeolian sediment transport is expressed in terms of local sediment availability without the need for spatial aggregation (de Vries et al., 2014b; Hoonhout and de Vries, 2016b). Such approach would require detailed measurements on spatiotemporal variations in aeolian sediment availability.

This paper presents detailed measurements of aeolian sediment transport rates from the Sand Motor during a six week field campaign in the fall of 2014. Spatial differences in sediment transport rates reveal the main erosion and deposition areas of aeolian sediment. Temporal variations in aeolian sediment transport are still expected to be correlated with the wind speed, but spatial variations are expected to be correlated with local variations in sediment availability. Understanding local sediment availability ultimately helps improving gross aeolian sediment transport estimates in availability-limited coastal systems.

2. Field Site

The Sand Motor mega nourishment was constructed in 2011 along the Delfland coast in The Netherlands (Figure 1, Stive et al., 2013). The Delfland coast was originally characterized by an alongshore uniform profile with an average dune height of 13 m, a dune foot at about 5 m+MSL and a beach slope of about 1:40.

The Sand Motor is constructed as a 21 Mm^3 hook-shaped peninsula that initially protruded about 1 km into the sea and stretched over approximately 2 km alongshore. The original crest height of the Sand Motor was on average about 5 m+MSL and locally 7 m+MSL; both are well above common surge level. Consequently, a significant part of the Sand Motor is uniquely shaped by aeolian processes that redistribute significant amounts of sediments within the Sand Motor region (Hoonhout and de Vries, 2016a).

Sand used for construction of the Sand Motor is medium sand with a median diameter of about 350 μm. The sand is obtained from an offshore borrowing pit in the North Sea and contains many shells and some pebbles, cobbles and other non-erodible material.

The predominant wind direction is south to southwest. Storms have a tendency to be oriented either southwest or northwest. Also the sediment transport potential (Ψ), defined as:

$$\Psi \propto \int u^3 \mathrm{d}t \tag{1}$$

in which u is the wind speed, is predominantly southwesterly or northwesterly oriented. The northwesterly storms are generally accompanied with
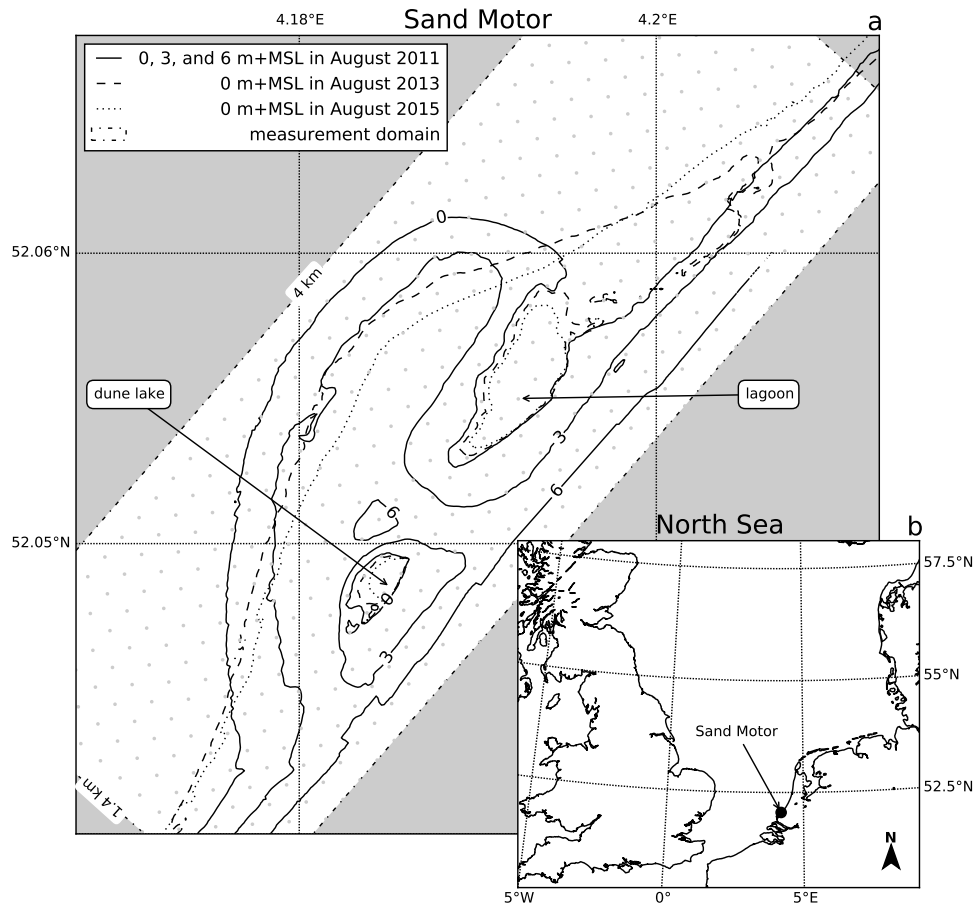
Figure 1: Location, orientation, appearance and evolution of the Sand Motor between construction 2011 and 2015. The box indicates the measurement domain used in the remainder of this paper. A 100 x 100 m grid aligned with the measurement domain is plotted in gray as reference.
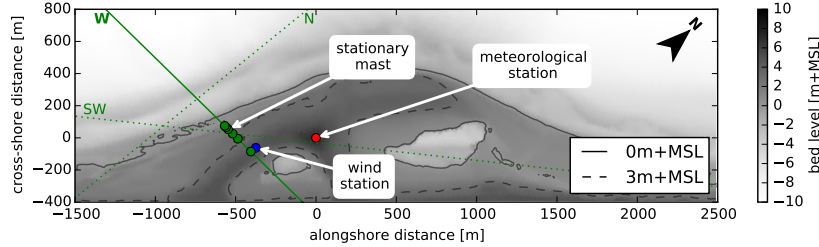
Figure 2: Overview of measurement transects N, W, and SW and locations during the MEGAPEX field campaign.

significant surges as the North Sea is virtually unbounded in northwesterly direction (Figure 1b).

The contour of the Sand Motor changed significantly in the four years after construction. Tidal forces diffuse about 1 Mm^3 per year along the coast (de Schipper et al., 2016). Four years after construction, the peninsula protrudes about 800 m into the sea and stretches over 4 km alongshore (Figure 1).

The Sand Motor provides a unique opportunity to perform measurements on spatial variations in aeolian sediment availability and transport. It accommodates vast and armored beaches next to dynamic intertidal beaches of varying width, while limitations in fetch are negligible.

3. Methodology

Sediment transport measurements were performed to investigate the role of the southern intertidal beaches as supplier of aeolian sediment in the Sand Motor region (Hoonhout and de Vries, 2016a). The change in sediment transport in downwind direction (spatial gradient) was measured along cross-shore transects running from the water line until the dry beach at approximately 5 m+MSL. Spatial gradients in saltation transport are positive in areas with net erosion and negative in areas with net deposition of sediment. The measurements were performed during the six week field campaign MEGAPEX (Mega Perturbation EXperiment) from September 17, 2014 until October 23, 2014.
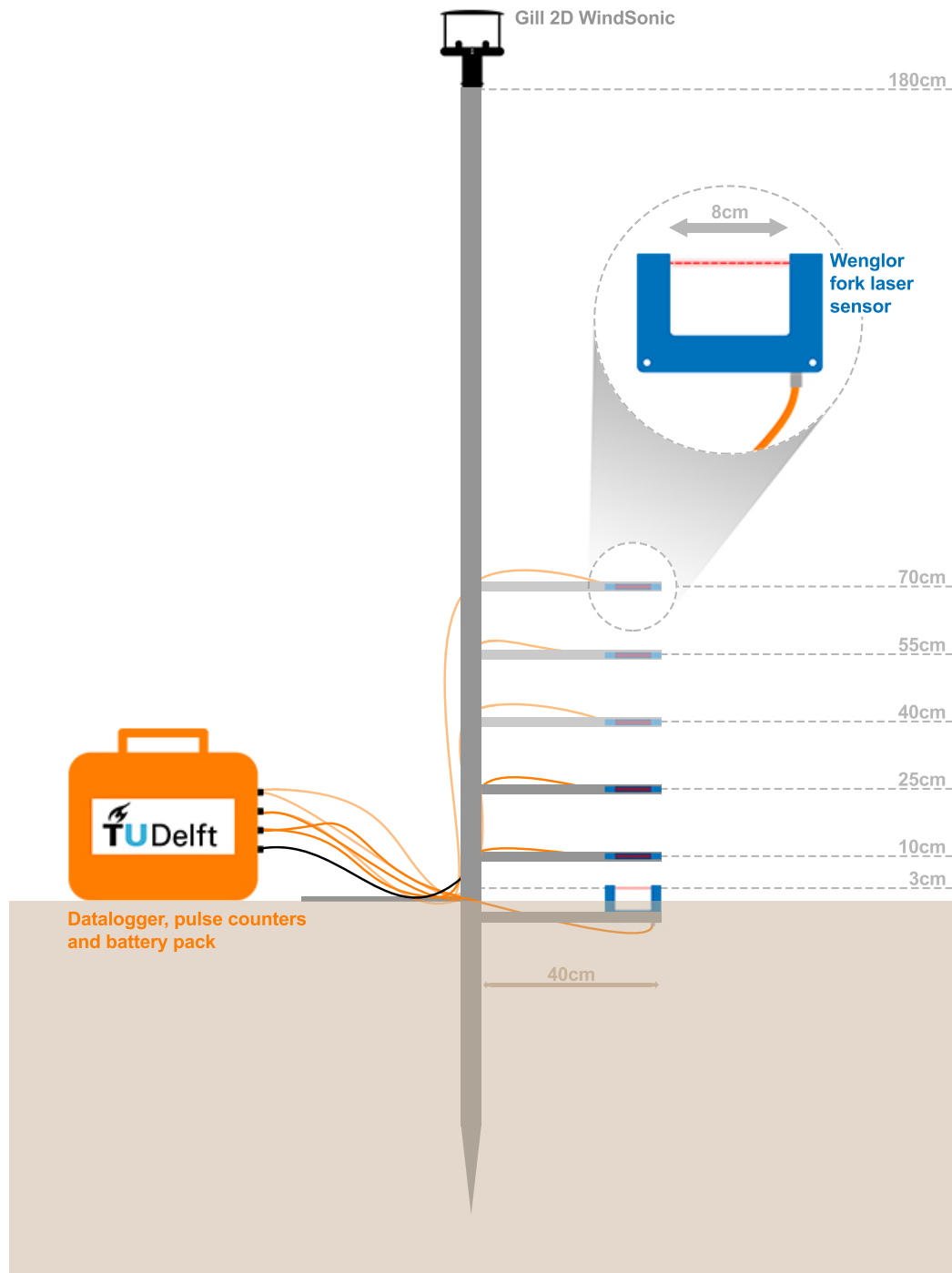
Figure 3: Mast with 6 Wenglor fork laser sensors and a Gill 2D WindSonic ultrasonic wind speed and direction sensor viewed in direction of the wind. The top 3 laser sensors are optional.

3.1. Equipment

The measurement set-up consists of 8 masts with battery power and data loggers. Each mast was equipped with at least three Wenglor fork laser sensors (P/N: YH08PCT8) for saltation measurements at 3, 10 and 25 cm above the bed (Figure 3). An additional three laser sensors were added to the most landward mast at 40, 55 and 70 cm above the bed to estimate the amount of particles bypassing the lower three sensors. Other masts could be equipped with three additional laser sensors as well. All except the lowest sensor were placed horizontally with the arms directed towards the wind as to minimize the disturbance of the wind field. The lowest sensor was placed vertically with the arms directed upwards, and partially buried as to further minimize the disturbance of the wind field. The Wenglor fork laser sensors register passing particles of 50 μm and larger with a frequency of 10 kHz using a laser beam of 0.6 mm. As the particle count is linearly related to the sediment flux (Hugenholtz and Barchyn, 2011), both are used indiscriminately in this study. The particle count is accumulated by a HOBO pulse counter (P/N: S-UCC-M001). A HOBO Energy data logger (P/N: H22-001) logged all sensors, including the pulse counters, at 1 Hz. In addition, three masts were equipped with a Gill 2D WindSonic ultrasonic wind speed and direction sensor (P/N: 1405-PK-040) at a height of 180 cm above the bed.

The masts can be rotated, but are not self-rotating to the wind as the masts were relocated depending on the wind direction. One stationary mast was present during almost the entire field campaign (Figure 2).

A separate Eijkelkamp wind station with three cup anemometers (P/N: 16.98.31) at heights 50, 100 and 180 cm and a wind vane (P/N: 16.98.34) at height 180 cm was present at a stationary location at the high beach for the entire duration of the field campaign. A Campbell Scientific meteorological station was present at the heart of the Sand Motor providing measurements on precipitation, humidity, solar radiation and wind speed and direction (Figure 2).

Qualitative small scale measurements on bed level change were performed by pressing erosion pins (nails) in the beach with falling tide. The erosion pins were placed along a cross-shore transect and about 10 cm apart with their heads flush to the bed. The erosion around the pins was measured manually with a ruler at the onset of flood.

Daily topographic surveys are performed along cross-shore transects using a Leica Viva GS10 RTG-GPS receiver. Offshore water levels and wave heights are obtained from gauges at the permanent offshore Europlatform.

3.2. Deployments

The measurement masts were deployed continuously during the field campaign, but have been relocated according to the governing wind direction. An overview of the measurement locations is given in Figure 2.

A single measurement transect consists of at least four masts: two in the intertidal beach area in order to capture the entrainment rate from the assumed sediment source region, one above the high water mark to capture the sediment flux from the intertidal beach area onto the dry upper beach and one higher up the beach to capture any additional sediment supply from the dry beach itself.

Table 1 lists the partitioning of the field campaign in 10 deployments with constant location and orientation of the measurement equipment. Most deployments were located along the westerly transect at the southern flank of the Sand Motor (Figure 2). Deployments DN02a and DN06a were aligned along alternative transects concurrent with deployments DN02b and DN06b respectively. During deployment DN11 all masts were clustered at high grounds as to provide a safe buffer from the expected surge during the storm event of October 23. Consequently, no transport gradients were measured during deployment DN11.

Table 1: Deployments of measurement masts during the MEGAPEX field campaign. Maximum measured wind speeds are in between brackets.

	wind speed	wind dir.	laser dir.	transect	duration	sensors	well oriented*
	[m/s]	[^{o}]	[^{o}]		[h]	[-]	[%]
DN02a	3 (10)	358	262	W	22	3	0
DN02b	3 (10)	359	360	N	22	3	100
DN04	5 (13)	343	360	W	42	3	92
DN05	3 (15)	196	270	W	312	3	40
DN06a	5 (17)	166	225	SW	170	3	55
DN06b	5 (17)	180	225	W	170	3	77
DN08	5 (16)	199	225	W	160	6	89
DN09	9 (21)	240	270	W	32	6	87
DN10	15 (22)	301	315	W	9	6	100
DN11	10 (24)	322	315	-	25	6	44

* The last column indicates the percentage of time in which the laser sensors were well oriented with respect to the wind. Raw data from all deployments is publishes as Hoonhout et al. (2016). DN01 is omitted from this list as it involved a test run of the equipment only. DN02a is listed only for convenience when interpreting the published dataset. DN02b and DN06b were originally named DN03 and DN07 respectively and can be found by these names only in the published dataset.

3.3. Data analysis

Particle count time series obtained from individual Wenglor laser sensors are summed up

1. per mast, to obtain *per-mast* particle count time series for each measurement mast, and
2. over all masts, to obtain *overall* particle count time series over all measurement masts.

The per-mast particle counts are totaled rather than averaged, and therefore not corrected for the number of Wenglor laser sensors per mast. All masts deployed simultaneously in a single transect were equipped with an equal number of sensors. Only the most landward mast in the westerly transect was permanently equipped with six sensors. However, the upper three sensors of the latter mast registered negligible particle counts. Averaging would result in approximately halving the per-mast particle counts. The halving of the particle count does not reflect any physical behavior and is therefore averted. Particle count time series are interchangeably referred to as particle count rates as the measurement interval was 1 Hz.

The overall particle count time series are used for comparison with the governing wind speed. For comparison with the wind direction per-mast particle count time series are discretized in bins according to the governing wind direction and subsequently summed over time. Also for comparison with water and bed levels, the per-mast particle count time series are discretized in bins and summed over time. Discretization is then done according to the global water level and local bed level at the measurement location.

Horizontal gradients in particle counts are computed from the per-mast particle count time series and the distance between the measurement masts. Vertical distributions in particle counts are computed from the per-sensor particle count time series for each measurement mast.

Particle counts are converted into sediment fluxes following Barchyn et al. (2014):

$$q_{\text{wenglor}} = n_{\text{wenglor}} \left(\frac{6 \cdot \gamma}{\rho \pi D^3} \cdot l_{\text{fork}} \cdot (l_{\text{laser}} + D) \right)^{-1} \tag{2}$$

with $\rho = 2650$ kg/m^3, $l_{\text{fork}} = 8 \cdot 10^{-2}$ m, $l_{\text{laser}} = 6 \cdot 10^{-4}$ m, $D = 335$ μm and $\gamma = 1$.

Variations in wind direction of more than 45° resulted in adjustment of the orientation of the Wenglor fork laser sensors. Particle counts with a discrepancy between wind direction and laser orientation ($\Delta\theta_u$) of more than 60° are considered not well oriented and are discarded from the presented

analysis. Other particle counts (n_{pc}) are corrected for orientation inaccuracies ($\hat{n}_{\text{pc}}$) using the basic geometric correction:

$$\hat{n}_{\text{pc}} = \frac{n_{\text{pc}}}{\cos(\Delta\theta_u)} \quad (3)$$

Periods without significant particle counts are not discarded from the analysis, except for the determination of the average wind direction as the wind direction tends to show random behavior for low wind conditions. The last column in Table 1 states the percentage of time in the laser sensors were well oriented with respect to the wind direction.

4. Results

The conditions during the field campaign were characterized by calm and sunny weather and negligible precipitation, which is unusual for the time of the year. The average wind speed over the entire experiment was 6 m/s (Figure 4a). The maximum wind speed was registered at 24 m/s at the end of the campaign on October 23 during the only measured storm event (DN10). The average overall particle count rate over the entire experiment was 120 s^{-1} or < 0.1 kg/m^2/s averaged over all deployed sensors (Figure 4b). The maximum overall particle count rate was registered on October 7 at 5800 s^{-1} or 4 kg/m^2/s (DN06b). Therefore, the maximum registered overall particle count rate did not coincide with the maximum wind speed.

The experiment covered two spring-neap cycles with a tidal range varying between 1.5 and 2.0 m (Figure 4c). The maximum still water level of 2.8 m+MSL was measured during storm deployment DN11 on October 22. This surge flooded the southern flank of the Sand Motor up to 5 m+MSL.

4.1. Relation between sediment transport and wind speed and water level

Periods with low wind conditions seem to coincide with periods with a negligible overall particle count, whereas periods with fair wind conditions seem to coincide with periods with a significant overall particle count (Figure 4a,b). Also the occurrence of peaks in overall particle count show a correspondence with peaks in wind speed. However, the highest peaks in wind speed do not necessarily coincide with the highest peaks in overall particle count, resulting in an overall poor correlation between wind speed and overall particle count (Figure 5a). The poor correlation is reflected in a Spearman rank correlation coefficient (Spearman, 1904) of zero, indicating that the data cannot be described by a monotonic function of any kind.

In the remainder of this paper it is shown that the storm deployments DN10 and DN11 provide signals with respect to wind direction, sediment
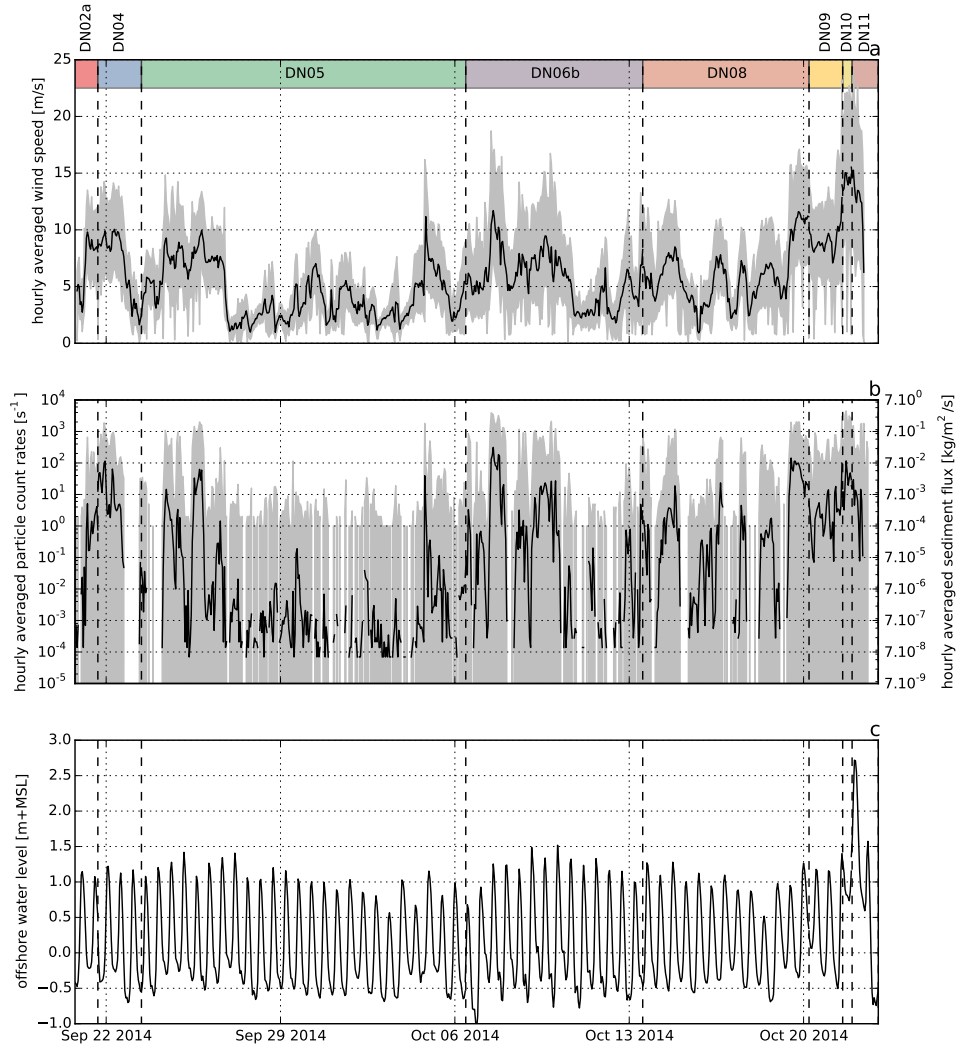
10

Figure 4: a) Wind time series, b) overall particle count rates during the deployments along the westerly transect, and c) offshore tidal elevation. Grey lines indicate the raw data, black lines the hourly averaged data. Colored bars refer to the deployments listed in Table 1. Deployments DN02b and DN06a are not included as these are located along different transects.
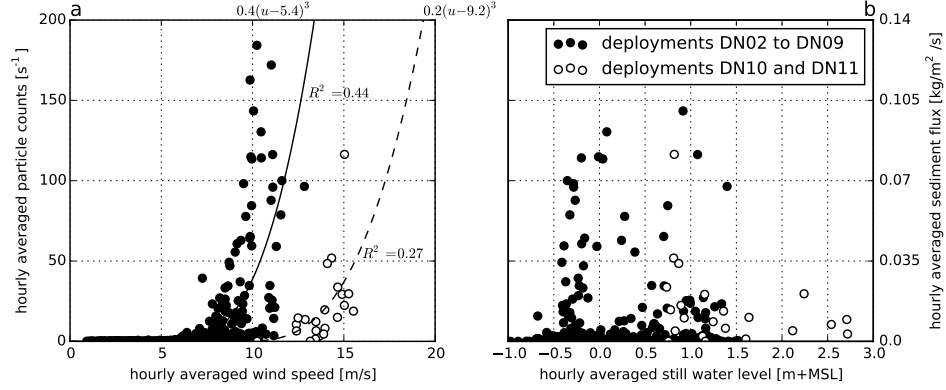
11

Figure 5: a) Relations between overall particle count and wind speed or b) water level. Closed circles and continuous lines refer to non-storm deployments DN02 to DN09. Open circles and dashed lines refer to storm deployments DN10 and DN11. All deployments are listed in Table 1.

availability and fetch that are consistently different from the non-storm deployments DN02 to DN09. In anticipation to these findings, correlations between wind speed and overall particle count are computed for the storm and non-storm deployments separately, resulting in a weak positive relation between wind speed and overall particle count. Fitting a third-power curve through these separate datasets results in R^2-values of 0.43 and 0.27 respectively. The low R^2-values indicate that much of the variance in the overall particle count is not explained by wind speed.

No relation between the still water level and the overall particle count is found (Figure 5b). There is no evidence that the spring-neap modulation of the high water level of about 0.5 m influenced the overall particle count significantly.

4.2. Wind direction and sediment source areas

The vast majority of per-mast particle counts registered at the stationary mast, that was located at the high water line during almost the entire field campaign (Figure 2), was registered from a limited number of wind directions. These directions do not coincide with the prevailing wind direction or the wind direction with the largest transport potential (Figure 6a).

Figure 6a shows that the prevailing wind direction was south, but that the largest transport potential (Equation 1) came from the southwesterly and northwesterly directions. The per-mast particle count does not align with the prevailing wind direction or the directions with the largest transport potential as both the southerly and northwesterly wind directions did not induce a significant particle count.
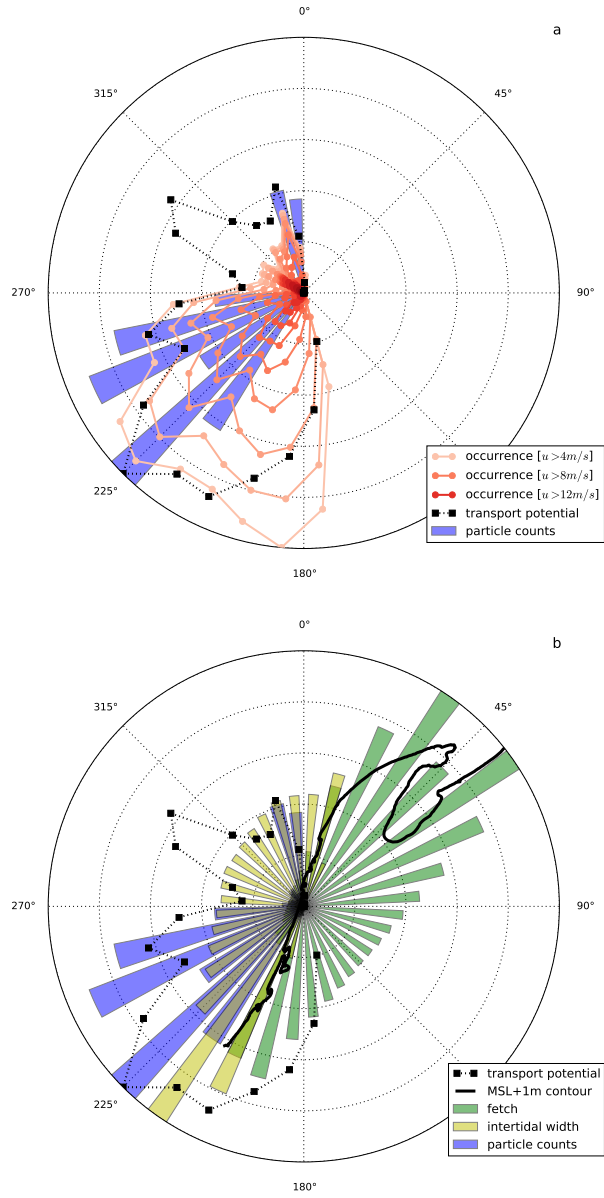
12

Figure 6: a) Per-mast particle count, wind speed and direction obtained from stationary mast (Figure 2) and b) available fetch and intertidal fetches.
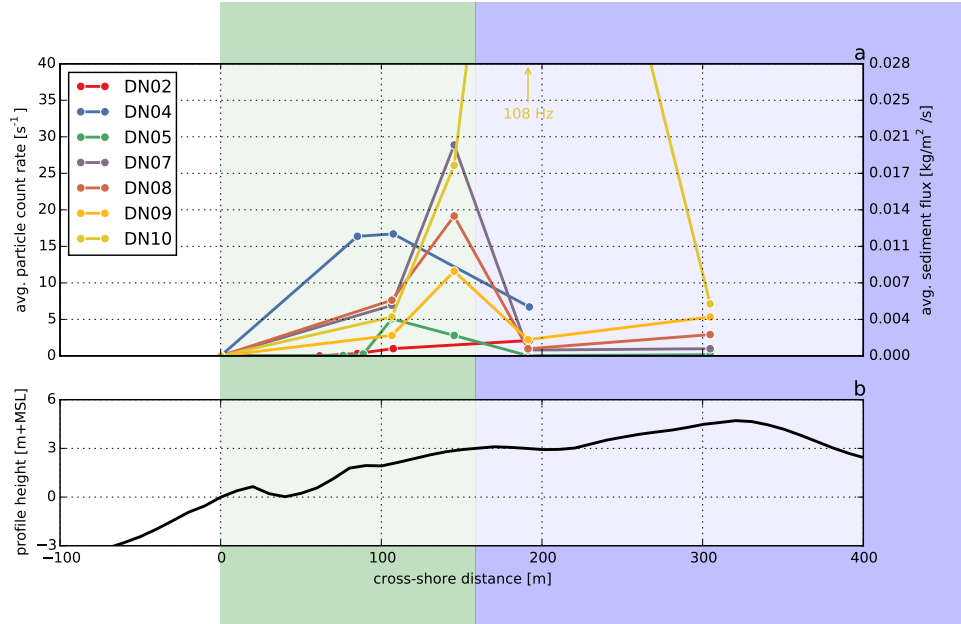
13

Figure 7: a) Average per-mast particle count rates during the deployments along the westerly transect and b) beach profile at the beginning of the field campaign. Line colors refer to the partitioning of the time series in Figure 4.

Figure 6b shows that most particles are registered from the wind directions with the shortest fetches. However, these wind directions provide among the largest intertidal beach widths along the Dutch coast. The exception is the northwesterly wind direction, that does accommodate a fair intertidal beach width, but did not register a per-mast particle count close to what could be expected from the transport potential. The northwesterly wind directions were solely present during the storm deployment DN10.

4.3. Spatial gradients in sediment transport

Significant variations in per-mast particle count along the measurement transects is found. Figure 7 shows that the largest increase in per-mast particle count in downwind direction (positive gradients) is consistently located in the intertidal beach area. Positive gradients in sediment transport indicate a net erosion of the beach surface and thus entrainment of sediment.

A significant decrease in per-mast particle count in downwind direction (negative gradients) is consistently found at the transition between intertidal and dry beach. Negative gradients in sediment transport indicate net deposition of sediment. Only during storm deployment DN10 the negative gradients at the transition were absent and large positive gradients in both the intertidal and dry beach area were found (Figure 7).
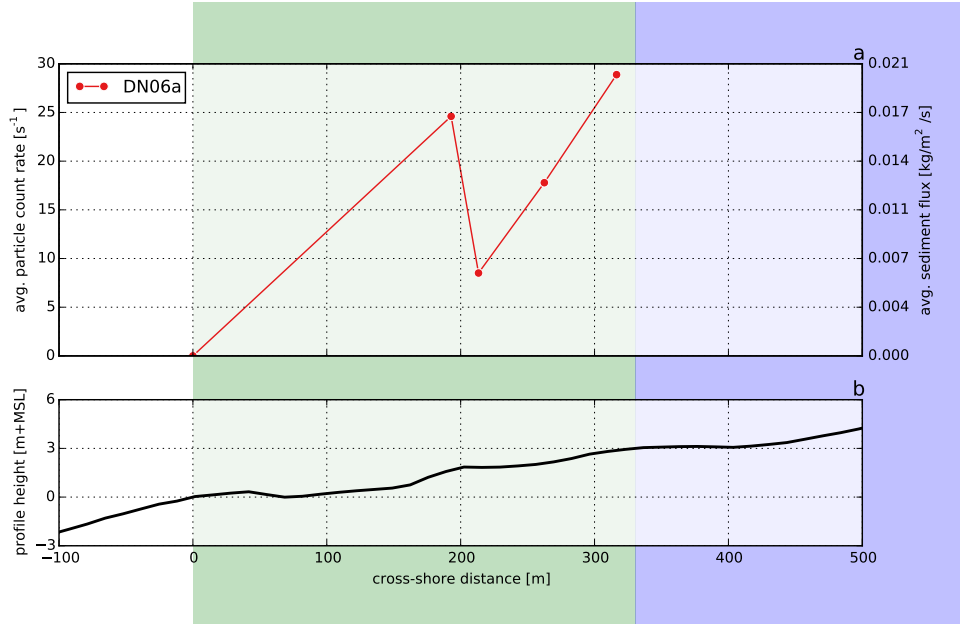
14

Figure 8: a) Average per-mast particle count rates during deployment DN06a along the southwesterly transect and b) beach profile at the beginning of deployment DN06.

The negative gradients coincide with the transition from the berm slope to the berm flat. Local deposition of aeolian sediment at the edge of a berm appears to be consistent behavior as it is also observed within the intertidal beach area. Four masts were deployed along a southwesterly transect within the intertidal beach area (DN06a, Figure 8) concurrent with deployment DN06b. These measurements show a significant decrease in per-mast particle count over a minor berm-like feature (x = 200 m) in the intertidal beach area. Downwind of this feature the per-mast particle count increased again with a rate comparable to what was found upwind of the berm-like feature. In addition, small scale measurements on bed level change confirm that erosion by wind is concentrated on the berm slope (Figure 9), while the berm flat tends to accrete. The maximum erosion of 1.2 cm in a single tidal cycle was measured with wind speeds above 10 m/s and little precipitation.

Measured negative gradients might also be caused by sediment locally bypassing the measurement equipment. To ensure that the number of bypassing particles is limited, the most landward mast in each transect was permanently equipped with six laser sensors up to 70 cm above the bed. The number of particles counted in the upper laser sensor was consistently low ($\leq 1\%$), suggesting that only a small number of particles bypassed the equipment at this point.
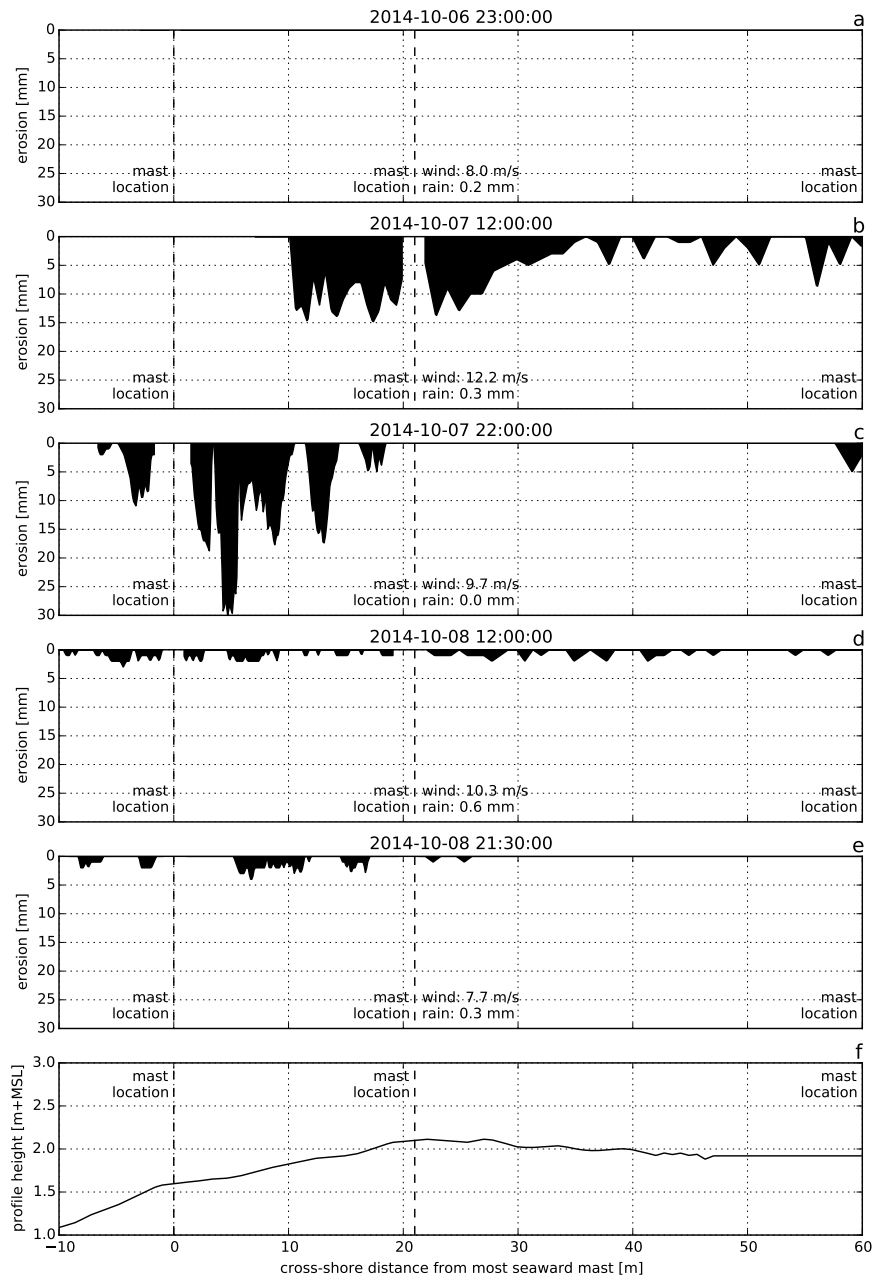
15

Figure 9: Erosion measured using erosion pins during five tidal cycles during deployment DN06a along the southwesterly transect. 16
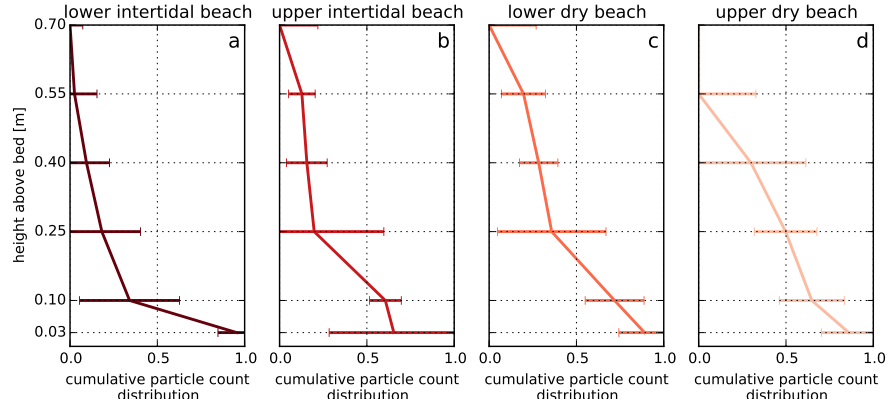
Figure 10: Cumulative particle count distribution over the vertical during deployment DN08. The line indicates the percentage of particles that bypasses a certain height above the bed. The horizontal bars visualize the variability in time of the particle count per laser sensor.

At the location downwind of the negative gradients more sediment might have bypassed than at the most landward measurement location. During deployment DN08 all four masts were equipped with six laser sensors in order to capture the vertical distribution of the particle count across the beach (Figure 10). It appears that the center of gravity of the particle count moves upward in downwind direction.Downwind of the negative transport gradient the percentage of particles counted by the upper laser sensor is 20% compared to $\leq 10\%$ at the other locations, suggesting that most particles bypassed at this location. The difference between the fraction of bypassing particles is too small to explain the large negative gradients, but are likely to cause the measured negative gradients to be overestimated.

4.4. Fetch vs. sediment availability

In Figure 11 the overall particle count obtained during the field campaign is binned according to the prevailing wind speed and the bed level at the measurement location. The average still water level is an indication of available fetch. The peak in overall particle count is at 3 m+MSL irrespective of the wind speed and available fetch. Therefore the overall particle count seems to be limited by location rather than wind speed or available fetch. The specific location at which the particle count peaks corresponds to the high water line and the onset of the shell pavement that largely covers the dry beach.
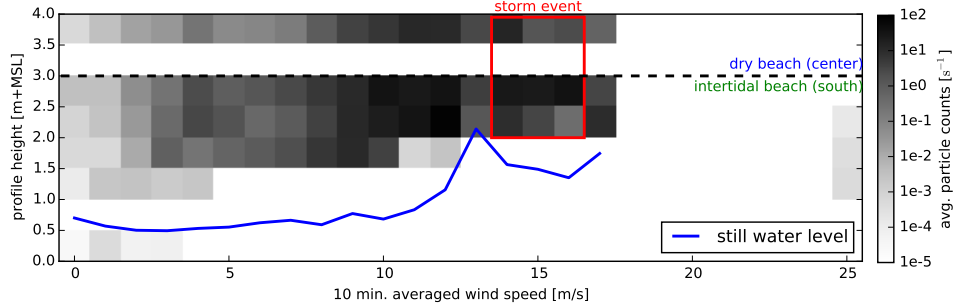
17

Figure 11: Average overall particle count rates depending on governing wind speed and bed level at measurement location, and average still water level depending on governing wind speed.

5. Discussion

The positive gradients in per-mast particle count in the intertidal beach area and minor positive gradients in the dry beach area suggest that the intertidal beach is a primary source of aeolian sediment in the Sand Motor region. This observation is in accordance with the large scale sediment budgets of the Sand Motor region (Hoonhout and de Vries, 2016a). Armoring of the dry beach surface, due to formation of lag deposits, might lead to a significant reduction in local aeolian sediment availability. Similarly, sediment availability might also be limited in the intertidal beach area due to periodic flooding and consequently high soil moisture contents. From the differences in per-mast particle count gradients between the intertidal and dry beach it can be assumed that the reduction of sediment availability due to armoring outweighs the influence of soil moisture. Local differences in bed surface properties would therefore induce relative differences in sediment availability that govern aeolian sediment transport in the Sand Motor region.

The negative gradients in per-mast particle count at the transition between intertidal and dry beach indicate that sediment eroded from the intertidal beach is deposited locally on the dry beach. Morphological feedback with the wind might cause the sediment transport capacity to peak at the berm edge due to the presence of a locally accelerated wind (i.e. jet flow; Hesp and Smyth, 2016), resulting in deposition at the berm flat. In addition, the berm edge coincides with the visually observed onset of a shell pavement (Figure 12). The shell pavement emerged from the nourished sediment in the first half year after construction of the Sand Motor (Hoonhout and de Vries, 2016a) due to winnowing of sand from the bed. Roughness elements, like
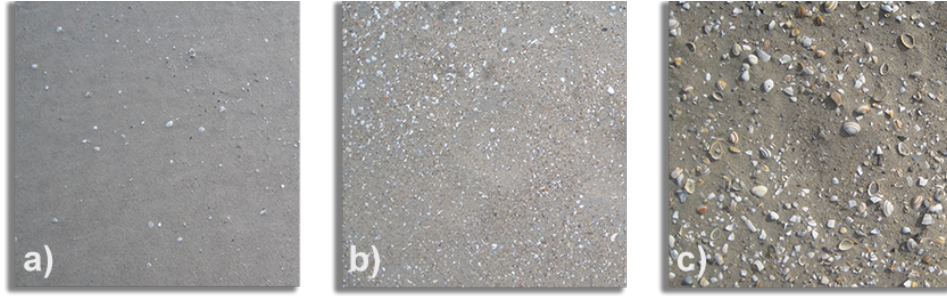
18

Figure 12: Visual impression of armor layer at three locations in the Sand Motor region: a) intertidal beach, no armoring b) lower dry beach, minor armoring with shell fragments c) upper dry beach, severe armoring with many shells and coarse sand. Covered surface is approximately 40 x 40 cm in all cases.
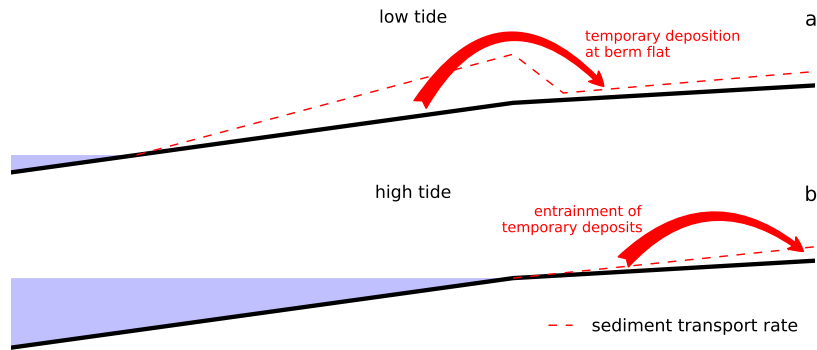

Figure 13: Conceptual illustration of how temporal deposits facilitate a continuous sediment supply from the intertidal beach to the dunes.

shells and cobbles, might trap impacting grains, and hamper saltation, or cause fully elastic collisions, and enhance saltation. The shell pavement at the measurement locations is relatively open and therefore both processes are likely to be relevant. The consistent negative gradients in particle count at the onset of the shell pavement suggest that trapping of sediment is dominant over the enhancement of saltation due to fully elastic collisions.

The local deposition of sediment at the berm flat is temporary as no accumulation of sand is observed on top of the shell pavement during the MEGAPEX field campaign. This suggests that sediment supply from marine sources and deposition in dunes, dune lake and lagoon is a phased process. In a phased system the local sediment deposits at the berm flat might act as temporary sediment source during high water (Figure 13). Consequently, measured aeolian sediment transport rates would be continuous and indepen-

19

dent of the instantaneous water level. The phasing of erosion and deposition can therefore explain the weak correlations between measured overall particle count and the instantaneous water level, which seemed to contrast the conclusion that the intertidal beach is a primary source of aeolian sediment.

The phasing of erosion and deposition increases the duration of transport from the intertidal beach to the dunes. The environmental conditions therefore needs to be favorable for aeolian sediment transport over a longer period for the sediment to reach the dunes. This requirement for dune growth closely relates to the need for synchronization between sediment availability and wind transport capacity emphasized by Houser (2009); Anthony (2013).

During a high wind event the relative importance of limitations in sediment availability might change. Strong winds can mobilize even the largest sediment fractions and shell fragments. Consequently, the beach armor layer itself might be transported and its reducing effect on sediment availability might be (partially) neutralized. Also the trapping of sediment due to an increase in bed roughness might be less effective and the influence of the berm on the wind flow reduced. In addition, high wind events are regularly accompanied with surges that prevent erosion of the intertidal beach by wind. Instead, the wind energy can be used for erosion of the dry beach, which contributes to the removal of the beach armor layer. The surge itself might also remove the beach armor layer by wave action or bury it by deposition of marine sediments. The removal or burial of the beach armor layer might elevate sediment availability from the dry beach also after the the storm passed. Only after development of a new beach armor layer the sediment availability and transport rates then equal the pre-storm situation.

The significant spatial variations in sediment transport gradients reflect significant variations in aeolian sediment availability. The formation of beach armor layers is known to limit aeolian sediment availability (McKenna Neuman et al., 2012) and cause spatial variations in aeolian sediment supply (Jackson et al., 2010). In case of the Sand Motor the formation of the beach armor layer is particularly accommodated by:

1. the high number of shells and other roughness elements that is generally contained by nourishment sand (van der Wal, 1998, 2000), and
2. the high construction height of the Sand Motor.

As the majority of the Sand Motor's subaerial surface has never been influenced by hydrodynamics, the beach surface in these areas is never reworked. Consequently, the majority of the Sand Motor's subaerial surface does not directly contribute to dune growth or beach-dune interactions (Houser and Ellis, 2013). The vast beach surface seems to stimulate dune growth only indirectly by sheltering the dunes from storm erosion.

Large scale nourishments are typically presented as natural solution to improve coastal safety. The natural dynamics of beach-dune systems depend on the periodic reworking of the beach surface as it prevents the formation of lag deposits. Large scale nourishments with a construction height above regular storm level can disrupt these natural dynamics as the formation of lag deposits is accommodated. The resulting compartmentalization of the beach can result in a phased process that decelerates dune growth and make dune growth more dependent on incidental storm events. Besides, also marine erosion would likely be limited, contributing to the lifetime of the nourishment. In contrast, limiting the construction height of large scale nourishments would reduce the lifetime of a nourishment, but result in a larger source area of aeolian sediment and the stimulation of dune growth and natural beach-dune interactions.

6. Conclusions

The Sand Motor (or Sand Engine) is a 21 Mm^3 mega nourishment along the Dutch coast that is constructed well above storm surge level (Stive et al., 2013) and therefore largely shaped by wind. During the six week MegaPex field campaign in the fall of 2014, spatial gradients in aeolian sediment transport were measured. The gradients identified the intertidal beach as the primary source of aeolian sediment. In addition, local temporal deposition of sediment at the berm flat occurred. The deposition is likely caused by a combination of morphological feedback with the wind and an increase in bed roughness due to the presence of a shell pavement. The local deposition of sediment causes the transport of sediment from intertidal beach to dunes, dune lake and lagoon to be phased.

From the measurements the following conclusions can be drawn:

1. In the Sand Motor region, the (southern) intertidal beach area is a more important source of aeolian sediment than the dry beach area.
2. The relative importance of the intertidal beach as supplier of aeolian sediment could be explained by the development of a beach armor layer in the dry beach area that outweighs the influence of high soil moisture contents in the intertidal beach area.
3. Aeolian sediment originating from the intertidal beach seems to settle on the berm flat and to be gradually transported further resulting in an continuous sediment flux from the intertidal beach area and into the dunes, even if the intertidal beach is flooded.

21

4. During high wind events, aeolian sediment availability in the intertidal beach area tends to be reduced by high water levels, while the sediment availability in the dry beach area tends to be increased due to mobilization of the beach armor layer;

5. The construction height of a mega nourishment is important to its lifetime as it is governs compartmentalization of the beach due to beach armoring.

Acknowledgements

References

Anthony, E. J. (2013). Storms, shoreface morphodynamics, sand supply, and the accretion and erosion of coastal dune barriers in the southern north sea. *Geomorphology*, 199:8–21. doi:10.1016/j.geomorph.2012.06.007.

Arens, S., Baas, A., Van Boxel, J., and Kalkman, C. (2001). Influence of reed stem density on foredune development. *Earth Surface Processes and Landforms*, 26(11):1161–1176.

Bagnold, R. (1937). The size-grading of sand by wind. *Proceedings of the Royal Society of London. Series A, Mathematical and Physical Sciences*, pages 250–264.

Barchyn, T. E., Hugenholtz, C. H., Li, B., McKenna Neuman, C., and Sanderson, S. (2014). From particle counts to flux: Wind tunnel testing and calibration of the "wenglor" aeolian sediment transport sensor. *Aeolian Research*, 15:311–318. doi:10.1016/j.aeolia.2014.06.009.

Bauer, B. O. and Davidson-Arnott, R. G. D. (2002). A general framework for modeling sediment supply to coastal dunes including wind angle, beach geometry, and fetch effects. *Geomorphology*, 49:89–108. doi:10.1016/S0169-555X(02)00165-4.

Bauer, B. O., Davidson-Arnott, R. G. D., Hesp, P. A., Namikas, S. L., Ollerhead, J., and Walker, I. J. (2009). Aeolian sediment transport on a beach: Surface moisture, wind fetch, and mean transport. *Geomorphology*, 105:106–116. doi:10.1016/j.geomorph.2008.02.016.

Belly, P. Y. (1964). Sand movement by wind. Technical Report 1, U.S. Army Corps of Engineers CERC, Vicksburg, MS. 38 pp.

Davidson-Arnott, R. G. D., MacQuarrie, K., and Aagaard, T. (2005). The effect of wind gusts, moisture content and fetch length on sand transport on a beach. *Geomorphology*, 68:115–129. doi:10.1016/j.geomorph.2004.04.008.

Davidson-Arnott, R. G. D., Yang, Y., Ollerhead, J., Hesp, P. A., and Walker, I. J. (2008). The effects of surface moisture on aeolian sediment transport threshold and mass flux on a beach. *Earth Surface Processes and Landforms*, 33(1):55–74. doi:10.1002/esp.1527.

de Schipper, M. A., de Vries, S., Ruessink, G., de Zeeuw, R. C., Rutten, J., van Gelder-Maas, C., and Stive, M. J. (2016). Initial spreading of a mega feeder nourishment: Observations of the sand engine pilot project. *Coastal Engineering*, 111:23–38. doi:10.1016/j.coastaleng.2015.10.011.

de Vries, S., Arens, S. M., de Schipper, M. A., and Ranasinghe, R. (2014a). Aeolian sediment transport on a beach with a varying sediment supply. *Aeolian Research*, 15:235–244. doi:10.1016/j.aeolia.2014.08.001.

de Vries, S., van Thiel de Vries, J. S. M., van Rijn, L. C., Arens, S. M., and Ranasinghe, R. (2014b). Aeolian sediment transport in supply limited situations. *Aeolian Research*, 12:75–85. doi:10.1016/j.aeolia.2013.11.005.

Delgado-Fernandez, I. (2010). A review of the application of the fetch effect to modelling sand supply to coastal foredunes. *Aeolian Research*, 2:61–70. doi:10.1016/j.aeolia.2010.04.001.

Dyer, K. R. (1986). *Coastal and estuarine sediment dynamics*. Wiley, Chichester.

Gillette, D. A. and Stockton, P. H. (1989). The effect of nonerodible particles on wind erosion of erodible surfaces. *Journal of Geophysical Research: Atmospheres*, 94(D10):12885–12893. doi:10.1029/JD094iD10p12885.

Hesp, P. A. and Smyth, T. A. G. (2016). Surfzone-beach-dune interactions: Flow and sediment transport across the intertidal beach and backshore. *Journal of Coastal Research*, SI 75:8–12. doi:10.2112/SI75-002.1.

Hoonhout, B. M. and de Vries, S. (2016a). Aeolian sediment supply at a mega nourishment. *Coastal Engineering*. Submitted.

Hoonhout, B. M. and de Vries, S. (2016b). A process-based model for aeolian sediment transport and spatiotemporal varying sediment availability. *Journal of Geophysical Research: Earth Surface.* doi:10.1002/2015JF003692. 2015JF003692.

Hoonhout, B. M., de Vries, S., and Cohn, N. (2016). Field measurements on aeolian sediment transport at the sand motor mega nourishment during the megapex field campaign. OpenDAP server. doi:10.4121/uuid:3bc3591b-9d9e-4600-8705-5b7eba6aa3ed.

Houser, C. (2009). Synchronization of transport and supply in beach-dune interaction. *Progress in Physical Geography*, 33(6):733–746. doi:10.1177/0309133309350120.

Houser, C. and Ellis, J. (2013). Beach and dune interaction. *Treatise on geomorphology. Academic, San Diego.* doi:10.1016/B978-0-12-374739-6.00283-9.

Howard, A. D. (1977). Effect of slope on the threshold of motion and its application to orientation of wind ripples. *Geological Society of America Bulletin*, 88(6):853–856. doi:10.1130/0016-7606(1977)88¡853:EOSOTT¿2.0.CO;2.

Hugenholtz, C. H. and Barchyn, T. E. (2011). Laboratory and field performance of a laser particle counter for measuring aeolian sand transport. *Journal of Geophysical Research*, 116(F1). doi:10.1029/2010JF001822. F01010.

Jackson, D. W. T. and Cooper, J. A. G. (1999). Beach fetch distance and aeolian sediment transport. *Sedimentology*, 46:517–522. doi:10.1046/j.1365-3091.1999.00228.x.

Jackson, N. L. and Nordstrom, K. F. (1998). Aeolian transport of sediment on a beach during and after rainfall, wildwood, nj, usa. *Geomorphology*, 22(2):151–157. doi:10.1016/S0169-555X(97)00065-2.

Jackson, N. L., Nordstrom, K. F., Saini, S., and Smith, D. R. (2010). Effects of nourishment on the form and function of an estuarine beach. *Ecological Engineering*, 36(12):1709–1718. doi:10.1016/j.ecoleng.2010.07.016.

Kocurek, G. and Lancaster, N. (1999). Aeolian system sediment state: theory and mojave desert kelso dune field example. *Sedimentology*, 46(3):505–515. doi:10.1046/j.1365-3091.1999.00227.x.

Lynch, K., Jackson, D. W., and Cooper, J. A. G. (2016). The fetch effect on aeolian sediment transport on a sandy beach: a case study from mag-illigan strand, northern ireland. *Earth Surface Processes and Landforms*. doi:10.1002/esp.3930.

McKenna Neuman, C., Li, B., and Nash, D. (2012). Micro-topographic analysis of shell pavements formed by aeolian transport in a wind tunnel simulation. *Journal of Geophysical Research*, 117(F4). doi:10.1029/2012JF002381. F04003.

Spearman, C. (1904). The proof and measurement of association between two things. *American Journal of Psychology*, 15:72–101. doi:10.2307/1412159.

Stive, M. J. F., de Schipper, M. A., Luijendijk, A. P., Aarninkhof, S. G. J., van Gelder-Maas, C., van Thiel de Vries, J. S. M., de Vries, S., Henriquez, M., Marx, S., and Ranasinghe, R. (2013). A new alternative to saving our beaches from sea-level rise: the Sand Engine. *Journal of Coastal Research*, 29(5):1001–1008. doi:10.2112/JCOASTRES-D-13-00070.1.

van der Wal, D. (1998). The impact of the grain-size distribution of nourish-ment sand on aeolian sand transport. *Journal of Coastal Research*, pages 620–631.

van der Wal, D. (2000). Grain-size-selective aeolian sand transport on a nourished beach. *Journal of Coastal Research*, pages 896–908.

Wiggs, G. F. S., Baird, A. J., and Atherton, R. J. (2004). The dynamic effects of moisture on the entrainment and transport of sand by wind. *Geomorphology*, 59:13–30. doi:10.1016/j.geomorph.2003.09.002.